Dalton Transactions

PAPER

View Article Online
View Journal

Cite this: DOI: 10.1039/d6dt00232c

Synthesis of the $NaGa(S_{1-x}Se_x)_2$ solid solution from mechanically activated precursors

Louisiane Verger, *[a] Julien Trébosc, [b] Santhoshkumar Sundaramoorthy,[c] Amitava Choudhury, [c] Olivier Hernandez,[d] Eric Furet,[a] Sébastien Chenu,[a] David Le Coq,[a] Laurent Calvez[a] and Olivier Lafon [e]

Received 29th January 2026,
Accepted 22nd March 2026

DOI: 10.1039/d6dt00232c

rsc.li/dalton

$NaGaS_2$ and $NaGaSe_2$ are two recently discovered compounds that crystallize in the same structure type. In this work, $NaGa(S_{1-x}Se_x)_2$ (x = 0.5, 0.75 and 1) are prepared using an alternative synthesis route, mechanochemistry followed by heat treatment. Na_2S, Na_2Se, Ga_2S_3 and Ga_2Se_3 are milled in stoichiometric proportions. Differential scanning calorimetry, X-ray diffraction and solid-state nuclear magnetic resonance (^{23}Na and ^{71}Ga) show that the compounds after milling are composed of crystalline $NaGa(S_{1-x}Se_x)_2$ with an amorphous part. Annealing promotes the formation of crystalline $NaGa(S_{1-x}Se_x)_2$. A linear variation in the lattice parameters is observed, indicating that a solid solution is formed and that Se substitutes for S.

1. Introduction

The need for safer rechargeable batteries with higher power densities is driving the search for all-solid-state battery (ASSB) designs using solid-state electrolytes.[1] Furthermore, sodium-based inorganic ASSBs offer an alternative to lithium technologies for large-scale applications, thanks to their lower cost and the widespread availability of Na element. Solid-state electrolytes can be divided into four classes: β/β″-Al_2O_3, NASICON, complex hydrides and halides and finally sulfides.[2] The latter are widely studied due to their soft mechanical properties, which ensure good contact at electrolyte/electrode interfaces, low grain boundary resistance and higher ionic conductivity compared to their oxide counterparts.

Sulfide-based materials are generally synthesized in silica tubes sealed under vacuum, which poses two problems: the reactivity of sodium with silica and sulfur vapors. To overcome these problems, mechanochemistry is used, where precursors are milled at high energy, inducing a chemical reaction. Depending on the precursors and the milling conditions, the resulting material may be (i) amorphous, (ii) crystalline, or (iii) a composite with an amorphous part and a crystalline part. The synthesis route of amorphous sodium thiophosphates for solid-state electrolytes has been established through mechanochemistry by Noi *et al.*[3] Since then, many different Na^+ conducting sulfur-based materials have been obtained by mechanochemistry, such as Na_3BS_3,[4] Na_2S-In_2S_3,[5] Na_5AlS_4-Na_4SiS_4,[6] Na_6MgS_4[7] and Na_2CaSnS_4,[8] in amorphous or crystalline forms. The amorphous domain of a given system can be extended by the use of mechanochemistry compared to melt-quenching,[9] which could be due to a higher quenching rate when the beads impact the powder.[10] Heat treatments can be employed as a second step for the amorphous material to promote crystallization. In general, the crystalline phase is the one obtained by conventional high-temperature synthesis.[11,12] However, for some specific compositions, metastable phases can be obtained,[13] such as $Li_7P_3S_{11}$ or Na_3PS_4.[14,15]

Recently, we used mechanochemistry to extend the amorphous domain of the pseudo-binary $x[Na_2S](100-x)[Ga_2S_3]$, with Na_2S content ranging from x = 20 to 80.[9] Crystalline $NaGaS_2$ was obtained by heating amorphous $NaGaS_2$ above its glass transition temperature.[11] In parallel, crystalline $NaGaS_2$ was synthesized for the first time by the flux method at 750 °C and 600 °C by Adhikary *et al.* and Klepov *et al.*[16,17] Sodium selenogallate $NaGaSe_2$ was later discovered, and it is isostructural to its sulfide analogue $NaGaS_2$.[18] They both crystallize in the $C2/c$ space group adopting a structure analogous to the $TlGaSe_2$ structure type. The structure is based on Ga_4S_{10} units connected by a bridging S atom, resulting in a layered structure. A representation of the structure can be found in SI, Fig. S1. The Ga_4S_{10} units are composed of two pairs of Ga_2S_7 connected through corner sharing. Na^+ ions are located in the

[a]Univ Rennes, CNRS, ISCR (Institut des Sciences Chimiques de Rennes) – UMR 6226, F-35000 Rennes, France. E-mail: louisiane.verger@univ-rennes.fr
[b]Univ. Lille, CNRS, INRAE, Centrale Lille, Univ. Artois, FR 2638 – IMEC – Fédération Chevreul, 59000 Lille, France
[c]Department of Chemistry, Missouri University of Science and Technology, Rolla, Missouri 65409, USA
[d]Nantes Université, CNRS, Institut des Matériaux de Nantes Jean Rouxel, IMN, F-44000 Nantes, France
[e]Univ. Lille, CNRS, Centrale Lille, Univ. Artois, UMR 8181 – UCCS – Unité de Catalyse et Chimie du Solide, 59000 Lille, France

valley formed by the Ga_4S_{10} units, in prisms with a triangular basis linked *via* their base to form chains. One out of every two prisms faces another prism of the upper plane, rotated by 90°. There are two inequivalent sites for both Na and Ga elements.

In this work, we use mechanochemistry followed by a thermal treatment to synthesise $NaGaSe_2$, along with intermediate compositions across the solid solution $NaGa(S_{1-x}Se_x)_2$ series.

2. Experimental

$NaGa(S_{1-x}Se_x)_2$ (x = 0.5, 0.75 and 1) were prepared by the mechanochemical method using a planetary ball mill Pulverisette 7 (Fritsch). Ga_2S_3 and Ga_2Se_3 were first synthesized. 8 g of stoichiometric mixture of gallium (Neyco, 99.99%) and sulfur (Strem Chemical Inc., 99.999%) or selenium (Umicore, 5N) was ball milled for 4 hours at 400 rpm in a tungsten carbide (WC) vessel (internal volume of 45 mL) with 10 WC balls (diameter 10 mm), resulting in a ball to powder mass ratio of 10 : 1.[19] Na_2Se was synthesized by taking stoichiometric amounts of Na and Se in liquid NH_3 following Birch reduction techniques.[20] The details of the synthesis can be found in the SI. Stoichiometric mixtures of Ga_2S_3, Ga_2Se_3, and Na_2S (Alfa Aesar, 95% purity) were weighed for $NaGa(S_{0.5}Se_{0.5})_2$. Stoichiometric mixtures of Ga_2Se_3 and Na_2S (Alfa Aesar, 95% purity) were weighed for $NaGa(S_{0.25}Se_{0.75})_2$. And finally, stoichiometric mixtures of Ga_2Se_3 and Na_2Se were weighed for $NaGaSe_2$. Each mixture was milled in zirconia pots (volume 45 mL), with zirconia balls (diameter 4 mm) and a 20 : 1 ball : powder mass ratio. The mass of the mixture was 5 g, and the rotational speed and milling duration were 600 rpm and 10 h, respectively. After 10 h of milling, the powders turned yellow. The synthesis of the $NaGaSe_2$ composition was performed twice to check the reproducibility of our method.

An annealing treatment was performed on powders obtained after mechanochemical treatment, pressed under 1.5 tons and under vacuum using a conventional uniaxial cold press to obtain a 1–1.5 mm thick pellet with a 10 mm diameter. The pellets were then heated in a silica tube sealed under vacuum, at their crystallization onset temperature T_x + 35 °C for 12 h. After annealing, the color of the powders becomes orange.

A DSC Q20 Thermal Analysis instrument was used to characterize the thermal properties of the synthesized materials. Measurements were performed from room temperature up to 500 °C with a heating rate of 10 °C min^{-1} on samples sealed under nitrogen in an aluminum crucible.

Conventional XRD measurements were performed on powders after different milling times to follow reaction processes on samples protected from air by a Kapton (polyimide) window. The XRD patterns were recorded in the 5–65° 2θ range with a 0.0261° step size and a counting time of 400 s per step using a PANalytical X'Pert Pro diffractometer (Bragg–Brentano geometry, Cu-source, Ni-filter, K_α radiation, 40 kV, 40 mA, PIXcel 1D detector).

XRD data on powders obtained after the annealing process were recorded with a counting time of 1200 s per step and in a wider range (5–130° 2θ) on powdered samples protected from air using a polycarbonate dome, which allows better airtightness. Le Bail profile refinements using the FullProf program were carried out.[21]

Energy dispersive spectroscopy (EDS) analyses were carried out on a JEOL JSM-IT 300 scanning electron microscope (SEM) using an acceleration voltage of 20 kV.

The nuclear magnetic resonance (NMR) experiments were carried out in the NMR facility of the advanced characterization platform of the Chevreul institute. Quantitative one-dimensional (1D) ^{23}Na and ^{71}Ga NMR spectra were acquired at a static magnetic field B_0 = 28.2 T using a Bruker BioSpin Avance NEO spectrometer and a narrow-bore hybrid NMR magnet built from both low-temperature and high-temperature superconductors equipped with a 1.3 mm double-resonance (HX) magic-angle spinning (MAS) probe.[22] The sodium-23 isotope is a spin-3/2 quadrupolar nucleus with a high natural abundance (NA) of 100%, and a moderate gyromagnetic ratio, $\gamma(^{23}Na) \approx 0.265\gamma(^{1}H)$, and electric quadrupolar moment, eQ, with Q = 10.4 fm^2, whereas for the ^{71}Ga isotope, NA = 39.89%, $\gamma(^{71}Ga) \approx 0.306\gamma(^{1}H)$ and Q = 10.4 fm^2.[23] All samples were packed into a zirconia rotor inside an argon-filled glovebox to prevent contact with moisture. The rotors were rotated at a MAS frequency of 50 kHz. The 1D ^{23}Na and ^{71}Ga NMR spectra were acquired using the Bloch-decay experiment with a pulse length (τ_p) of 1 μs and a radiofrequency (rf) field strength (ν_1) of 90 kHz for ^{23}Na, and τ_p = 0.475 μs and ν_1 = 128 kHz for ^{71}Ga. The 1D ^{23}Na and ^{71}Ga NMR spectra were obtained by averaging 512 and 1024 transients with a recycling delay of 3 s and 0.5 s for ^{23}Na and ^{71}Ga, respectively. The ^{1}H isotropic chemical shifts were referenced to tetramethylsilane (TMS) diluted at 1 vol% in $CDCl_3$ using the unresolved signal of adamantane at 1.73 ppm as a secondary reference. ^{23}Na and ^{71}Ga chemical shifts were indirectly referenced using the previously published relative NMR frequencies.[23]

3. Results and discussion

The reaction during the milling procedure is followed by XRD measurements acquired on the powder after every hour. As an example, Fig. 1a shows the copper-source XRD patterns of the composition $NaGa(S_{0.25}Se_{0.75})_2$ after 1, 2, 4, 6 and 10 h of milling the Na_2S and Ga_2Se_3 precursors. The diffraction halo between 15 and 25° 2θ is due to the Kapton window used to protect the sample from air. After 1 h and 2 h of milling, the sharp peaks of Na_2S and the broad peaks of Ga_2Se_3 are still detected, together with a new crystalline phase indicated by grey dots. After only 4 h of milling, the precursors are no longer detected, and additional peaks of the new phase are detected. The XRD patterns did not evolve between 6 and 10 h, so the mechanical process was stopped after 10 h. A similar evolution is observed for sample $NaGa(S_{0.5}Se_{0.5})_2$, presented in SI Fig. S3. For $NaGaSe_2$, also shown in Fig. S3 of the SI, the

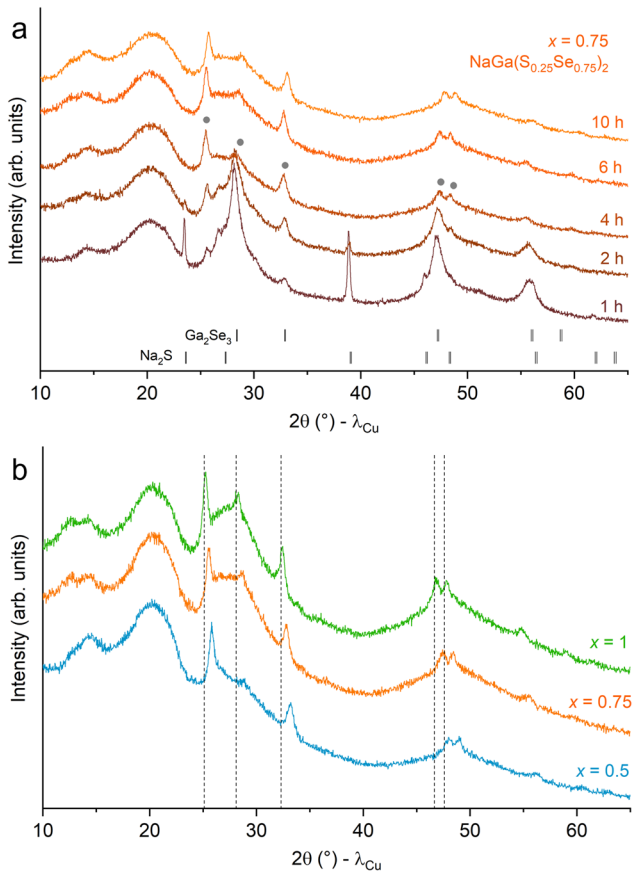

Fig. 1 (a) Powder Cu-XRD patterns of the $NaGa(S_{0.25}Se_{0.75})_2$ sample prepared by ball milling for different durations. The black vertical tick marks show Bragg positions of Na_2S and Ga_2Se_3. The grey dots correspond to crystalline $NaGa(S_{0.25}Se_{0.75})_2$. (b) Powder Cu-XRD patterns of the $NaGa(S_{1-x}Se_x)_2$ samples with x = 0.5 (blue), 0.75 (orange) and 1 (green) obtained after 10 h of milling. The vertical lines are a guide to the eye to see the shift of the peaks.

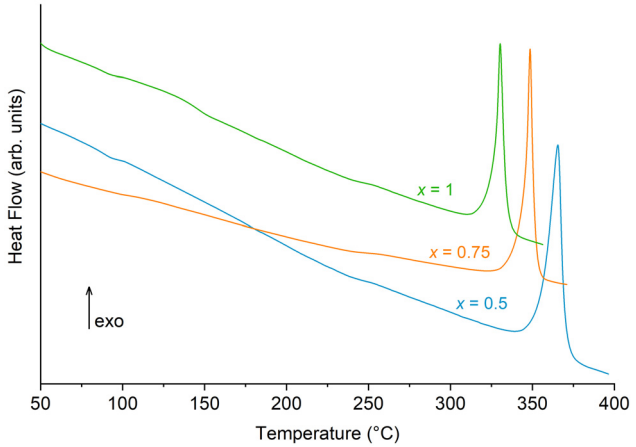

Fig. 2 DSC curve of the $NaGa(S_{1-x}Se_x)_2$ samples with x = 0.5 (blue), 0.75 (orange) and 1 (green) obtained after mechanical milling.

only difference is the formation of an intermediate crystalline phase at 1 h and 2 h of milling, which then reacts. This phase is not present in the precursors and remains unidentified.

Fig. 1b shows the copper-source XRD patterns of the $NaGa(S_{1-x}Se_x)_2$ (x = 0.5, 0.75 and 1) samples after 10 h of milling. The samples are poorly crystallized, with peaks that can be attributed to a unique $NaGa(S_{1-x}Se_x)_2$ crystalline phase. S can be substituted by Se in the $NaGaS_2$ structure and a solid solution therefore exists in the system $NaGa(S_{1-x}Se_x)_2$. The peaks are shifted towards lower angles as the Se content increases. Contrary to our previous work on $NaGaS_2$ (x = 0), amorphous powders were not obtained during the ball-milling process due to the crystallization of $NaGa(S_{1-x}Se_x)_2$ that could not be further totally amorphized. The samples are therefore a composite of a crystalline phase and an amorphous part.

Fig. 2 shows the DSC traces of the $NaGa(S_{1-x}Se_x)_2$ samples with x = 0.5 (blue), 0.75 (orange) and 1 (green) obtained after 10 h of milling. There was no clear evidence of the presence of a glass transition temperature attesting to the presence of a glass. However, a crystallization peak is detected, which shifted towards lower temperature with increasing Se content in the samples. In the literature, the substitution of S by Se also induces a decrease in crystallization temperature in the Ga–Ge–X and Ga–Sb–X systems, where X = S or Se.[24–27] The crystallization onset temperature (T_x) is 353, 334 and 322 °C (±2 °C) for x = 0.5, 0.75 and 1, respectively.

An annealing treatment was performed on the samples obtained after the mechanical milling at T_x + 35 °C for 12 h. The crystallization of $NaGa(S_{1-x}Se_x)_2$ is promoted by the thermal treatment, and $NaGa(S_{1-x}Se_x)_2$ is the only crystalline phase detected with higher crystallinity than before thermal treatment. For example, Fig. 3 shows the XRD pattern of $NaGaSe_2$ annealed for 12 h. The diffraction halo around 18° 2θ is due to the polycarbonate dome used to protect the sample from air. The experimental patterns differ from the calculated

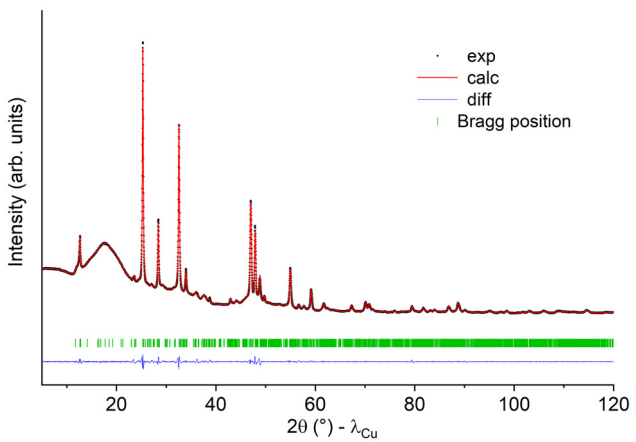

Fig. 3 Powder Cu-XRD pattern of $NaGaSe_2$ after annealing (black circles) and calculated profile using the Le Bail refinement method (χ^2 = 5, R_{wp} = 6.33%, R_p = 8.72%) (red line). The difference is drawn in blue and green bars correspond to the Bragg reflections for $NaGaSe_2$ from the structural model of Balijapelly *et al.*[18]

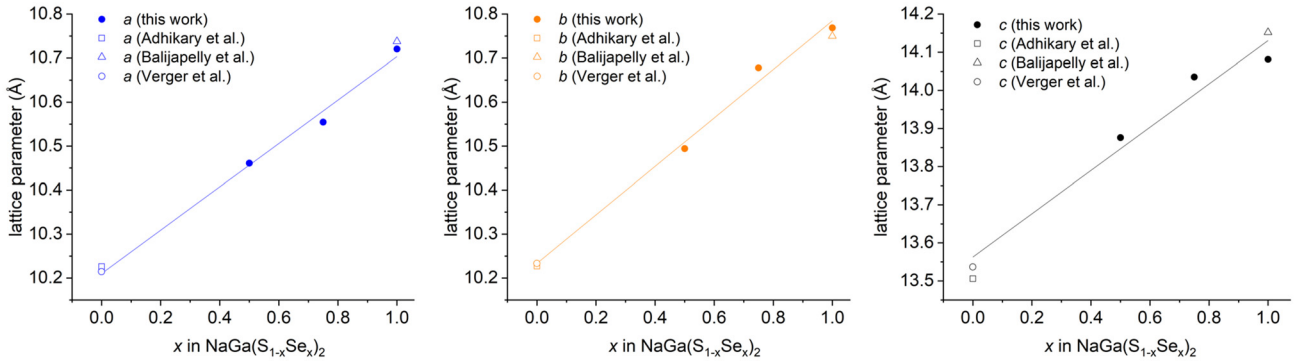

Fig. 4 From left to right: evolution of *a*, *b* and *c* lattice parameters as a function of *x* in $NaGa(S_{1-x}Se_x)_2$ (solid circles) synthesized in this work. The lines correspond to a linear fit using the data on compounds obtained by mechanochemistry from this work and from our previously published work on $NaGaS_2$[11] (R^2 = 0.99135, 0.99145, 0.96121 for *a*, *b* and *c*, respectively).

Table 1 Lattice parameters of $NaGa(S_{1-x}Se_x)_2$ (*x* = 0, 0.5, 0.75 and 1) from the literature and this work

Composition	$NaGaS_2$	$NaGaS_2$	$NaGa(S_{0.5}Se_{0.5})_2$	$NaGa(S_{0.25}Se_{0.75})_2$	$NaGaSe_2$	$NaGaSe_2$
Ref.	16	11	*This work*	*This work*	*This work*	18
a (Å)	10.226(3)	10.214(3)	10.461(2)	10.554(9)	10.721(8)	10.738(3)
b (Å)	10.227(3)	10.233(3)	10.494(1)	10.678(1)	10.769(9)	10.750(3)
c (Å)	13.506(5)	13.537(3)	13.876(2)	14.035(2)	14.081(1)	14.152(4)
β (°)	100.954(5)	101.054(2)	100.698(1)	100.669(6)	100.429(6)	100.954(5)

ones reported in the work of Adhikary *et al.*[16] and Balijapelly *et al.*[18] on $NaGaS_2$ and $NaGaSe_2$, respectively. This is due to the presence of stacking faults in the structure which greatly affect the intensity and broadening of some reflections, leading to apparent observed extinctions. Possibilities to perform a Rietveld refinement are then extremely limited, but profile refinements using the Le Bail method without structural constraints were carried out.

The refined lattice parameters of phases $NaGa(S_{1-x}Se_x)_2$ with *x* = 0.5, 0.75 and 1 using the C2/*c* space group are gathered in Fig. 4 and Table 1, together with data from the literature on $NaGaS_2$ and $NaGaSe_2$. As expected, the lattice parameters increase with the substitution of S by Se. *a* and *b* from $NaGaSe_2$ obtained by mechanochemistry and thermal treatment are close to those obtained by Balijapelly *et al.*[18] The *c* parameter is 0.07 Å lower in our work, meaning that the distance between the layers is lower. A linear regression points out that the solid solution $NaGa(S_{1-x}Se_x)_2$ obeys Vegard's law.

The composition of the samples before and after thermal treatment is verified by ESD measurements and presented in Table 2. The K_α radiation for Na (1.041 keV) and the L_α radiation for Ga (1.098 keV) are close in energy and are therefore difficult to distinguish. This introduces an error: for all samples, values obtained from the experimental quantitative analysis are significantly lower than the theoretical value for Na and higher than the theoretical value for Ga. However, the measurements still show that the composition of the samples before and after annealing is similar and that the S/Se ratio is correct.

NMR spectroscopy was used to probe local environments of Na and Ga atoms. The quantitative 1D ^{71}Ga spectra of the

Table 2 Theoretical composition and composition evaluated by EDS (±2 at%) of the $NaGa(S_{1-x}Se_x)_2$ sample after milling and after annealing

		Na (at%)	S (at%)	Ga (at%)	Se (at%)
x = 0.5	After milling	18	19	37	26
	After annealing	19	20	35	26
	Theoretical composition	*25*	*25*	*25*	*25*
x = 0.75	After milling	18	9	35	37
	After annealing	19	10	33	38
	Theoretical composition	*25*	*12.5*	*25*	*37.5*
x = 1	After milling	17	0	35	48
	After annealing	17	0	33	49
	Theoretical composition	*25*	*0*	*25*	*50*

samples before and after the annealing treatment are shown in Fig. 5. Overall, the spectra of the samples before the annealing treatment shown in dotted lines (just after the mechanochemical step) exhibit broader signals, indicating a distribution of local Ga environments typical of amorphous or poorly crystallized materials. The detected peaks become sharper after the annealing step, which leads to the crystallization of the materials and hence reduces the disorder. The ^{71}Ga NMR spectrum of $NaGa(S_{0.5}Se_{0.5})_2$ exhibits five peaks, which can be attributed to Ga atoms covalently bonded to different numbers of S and Se atoms: GaS_4, $GaSeS_3$, $GaSe_2S_2$, $GaSe_3S$ and $GaSe_4$. In our previous work on $NaGaS_2$, we showed that the [GaS_4] sites resonated at an isotropic chemical shift of around 318 ppm and the two crystallographically inequivalent GaS_4 sites are too similar to allow an unambiguous assignment.[11] The peak with the highest shift in the spectrum of $NaGa(S_{0.5}Se_{0.5})_2$ can then be attributed to Ga surrounded by

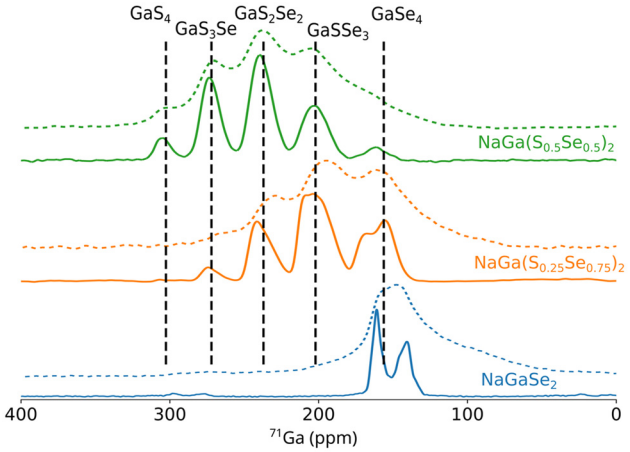

Fig. 5 Quantitative 1D ^{71}Ga MAS NMR spectra of $NaGa(S_{1-x}Se_x)_2$ before (dashed line) and after the annealing treatment (solid line) acquired at 28.2 T.

four S. As S is replaced by Se in the $[GaX_4]$ tetrahedron, the isotropic chemical shift of ^{71}Ga nuclei towards lower values occurs, down to about 170 ppm for $[GaSe_4]$. Contrary to $NaGaS_2$, two distinct peaks are detected for $NaGaSe_2$ after the thermal treatment, meaning that the two inequivalent sites for Ga can be distinguished.

The quantitative 1D ^{23}Na MAS NMR spectra of the investigated samples are displayed in Fig. 6. The spectra of $NaGa(S_{0.5}Se_{0.5})_2$ before the thermal treatment (dotted green line in Fig. 6) are composed of two broad signals, one more intense at a higher chemical shift (4.3 ppm) and a smaller contribution at a lower chemical shift (−6.1 ppm). After annealing, the spectrum is composed only of the contribution at a lower chemical shift, which becomes sharper. This change was also observed in our previous work on $NaGaS_2$.[11] We can then conclude that the contribution at −6.1 ppm stems from the crystalline $NaGa(S_{0.5}Se_{0.5})_2$ phase, with the two inequivalent crystallographic Na sites overlapping, whereas the contribution at 4.3 ppm comes from the amorphous phase. This assignment is in agreement with the XRD and DSC results, confirming that $NaGa(S_{0.5}Se_{0.5})_2$ before the thermal treatment is a composite of a crystalline phase and an amorphous part. Similar observations can be made on $NaGa(S_{0.25}Se_{0.75})_2$ before the thermal treatment (dotted orange lines in Fig. 6), with the peak at 3.6 ppm attributed to the amorphous phase and the peak at −5.0 ppm assigned to the crystalline $NaGa(S_{0.25}Se_{0.75})_2$ phase. After the thermal treatment, one main signal centered at −7 ppm is detected, subsuming several contributions. The shoulder at −2.5 ppm probably corresponds to a residual amorphous phase. Finally, for the sample $NaGaSe_2$ before thermal treatment, the spectrum is composed of one main contribution at 3.5 ppm, corresponding to amorphous $NaGaSe_2$, and two contributions at a high chemical shift, −4.8 and −10 ppm. After crystallization, the spectrum is characterized by four peaks, while only two inequivalent sites for Na are reported in the structure. The synthesis was performed a second time, and the same spectrum was obtained. The reason for the different features is still under investigation.

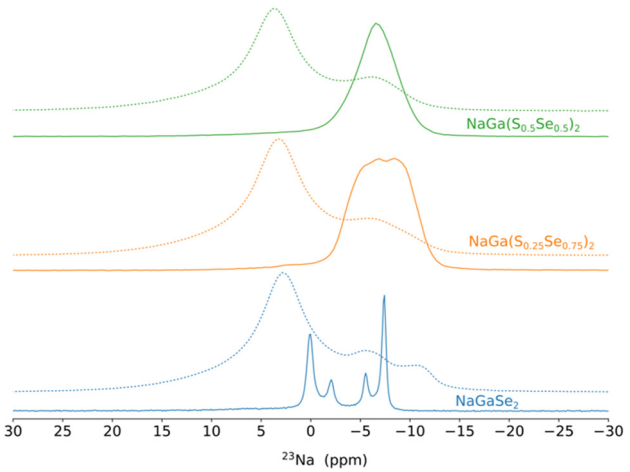

Fig. 6 Quantitative 1D ^{23}Na MAS NMR spectra of $NaGa(S_{1-x}Se_x)_2$ before (dashed line) and after the annealing treatment (solid line).

4. Conclusion

$NaGa(S_{1-x}Se_x)_2$ (x = 0.5, 0.75 and 1) was obtained by mechanochemistry. After 10 h of milling, the synthesized samples were characterized by XRD showing diffraction halos characteristic of amorphous materials, together with the presence of crystalline $NaGa(S_{1-x}Se_x)_2$. The DSC traces show the presence of a crystallization peak, whose temperature decreases with increasing Se content. ^{23}Na NMR measurements confirmed the presence of crystalline and amorphous $NaGa(S_{1-x}Se_x)_2$ in the samples. An annealing treatment at T_x + 35 °C was performed. This promotes the crystallization of $NaGa(S_{1-x}Se_x)_2$. A linear variation of the lattice parameters is observed, which means that a solid solution is formed. Milling acts here as an activation step to promote the crystallization of $NaGa(S_{1-x}Se_x)_2$ at lower temperatures compared to those of classical synthesis in a sealed silica tube.

Conflicts of interest

There are no conflicts to declare.

Data availability

The data supporting this article are available within the article, in the supplementary information (SI) and from the corresponding author upon request.

Supplementary information is available. See DOI: https://doi.org/10.1039/d6dt00232c.

Acknowledgements

This publication is (partially) supported by the European Union through the European Regional Development Fund (ERDF), the Ministry of Higher Education and Research, the French region of Brittany and Rennes Métropole. The Chevreul Institute is thanked for supporting CPER projects funded by the "Ministère de l'Enseignement Supérieur et de la Recherche", the region "Hauts-DEER-France", the ERDF program of the European Union and the "Métropole Européenne de Lille". Financial support from the IR INFRANALYTICS FR2054 for conducting the research is gratefully acknowledged. We are grateful to Z. Barbotin for her help with the EDS measurements.

References

1 M. Armand and J. M. Tarascon, Building better batteries, *Nature*, 2008, **451**, 652–657.
2 Y. Yang, *et al.*, Inorganic All–Solid–State Sodium Batteries: Electrolyte Designing and Interface Engineering, *Adv. Mater.*, 2024, **36**, 2308332.
3 K. Noi, A. Hayashi and M. Tatsumisago, Structure and properties of the Na_2S–P_2S_5 glasses and glass–ceramics prepared by mechanical milling, *J. Power Sources*, 2014, **269**, 260–265.
4 F. Tsuji, *et al.*, Preparation and characterization of sodium-ion conductive Na_3BS_3 glass and glass–ceramic electrolytes, *Mat. Adv.*, 2021, **2**, 1676–1682.
5 K. Motohashi, *et al.*, Sodium-Ion Conducting Solid Electrolytes in the Na_2S–In_2S_3 System, *Electrochemistry*, 2022, **90**, 067009.
6 S. Harm, *et al.*, Finding the Right Blend: Interplay Between Structure and Sodium Ion Conductivity in the System Na_5AlS_4–Na_4SiS_4, *Front. Chem.*, 2020, **8**.
7 H. Ben Yahia, K. Motohashi, A. Sakuda and A. Hayashi, Mechanochemical Synthesis and Structure of the Alkali Metal Magnesium Chalcogenide Na_6MgS_4, *Inorg. Chem.*, 2023, **62**, 10440–10449.
8 H. Ben Yahia, A. Sakuda and A. Hayashi, Mechanochemical synthesis of rock salt-type Na_2CaSnS_4 as a sodium-ion conductor, *RSC Mechanochem.*, 2025, **2**, 159–164.
9 K. Dénoue, *et al.*, New synthesis route for glasses and glass-ceramics in the Ga_2S_3-Na_2S binary system, *Mater. Res. Bull.*, 2021, **142**, 111423.
10 B. Xue, L. Calvez, M. Allix, G. Delaizir and X. H. Zhang, Amorphization by Mechanical Milling for Making IR Transparent Glass–Ceramics, *J. Am. Ceram. Soc.*, 2016, **99**, 1573–1578.
11 L. Verger, *et al.*, Mechanochemical synthesis and study of the local structure of $NaGaS_2$ glass and glass-ceramics, *Inorg. Chem.*, 2022, **61**, 18476–18485.
12 C. Fritsch, A. L. Hansen, S. Indris, M. Knapp and H. Ehrenberg, Mechanochemical synthesis of amorphous and crystalline $Na_2P_2S_6$-elucidation of local structural changes by X-ray total scattering and NMR, *Dalton Trans.*, 2020, **49**, 1668–1673.
13 X. Zhi and A. R. West, Mechanosynthesis of Disordered Rock Salt Structures: Thermodynamic and Kinetic Considerations, *Chem. Mater.*, 2023, **35**, 6790–6798.
14 F. Mizuno, A. Hayashi, K. Tadanaga and M. Tatsumisago, New Highly Ion-Conductive Crystals Precipitated from Li_2S-P_2S_5 Glasses, *Adv. Mater.*, 2005, **17**, 918–921.
15 A. Hayashi, K. Noi, A. Sakuda and M. Tatsumisago, Superionic glass-ceramic electrolytes for room-temperature rechargeable sodium batteries, *Nat. Commun.*, 2012, **3**, 856.
16 A. Adhikary, *et al.*, Unusual Atmospheric Water Trapping and Water Induced Reversible Restacking of 2D Gallium Sulfide Layers in $NaGaS_2$ Formed by Supertetrahedral Building Unit, *Chem. Mater.*, 2020, **32**, 5589–5603.
17 V. V. Klepov, *et al.*, $NaGaS_2$: An Elusive Layered Compound with Dynamic Water Absorption and Wide–Ranging Ion–Exchange Properties, *Angew. Chem., Int. Ed.*, 2020, **59**, 10836–10841.
18 S. Balijapelly, *et al.*, $NaGaSe_2$: A Water-Loving Multifunctional Non-van der Waals Layered Selenogallate, *Inorg. Chem.*, 2023, **62**, 3886–3895.
19 K. Dénoue, *et al.*, Mechanochemical synthesis and structural characterization of gallium sulfide Ga_2S_3, *J. Solid State Chem.*, 2020, **292**, 121743.
20 I. Schewe-Miller, *Metallreiche Hauptgruppenmetall-Chalkogenverbindungen: Synthese, Strukturen und Eigenschaften*. (na, 1990).
21 J. Rodríguez-Carvajal, Recent advances in magnetic structure determination by neutron powder diffraction, *Phys. B*, 1993, **192**, 55–69.
22 P. Wikus, W. Frantz, R. Kümmerle and P. Vonlanthen, Commercial gigahertz-class NMR magnets, *Supercond. Sci. Technol.*, 2022, **35**, 033001.
23 R. K. Harris, E. D. Becker, S. M. C. De Menezes, R. Goodfellow and P. Granger, NMR nomenclature: Nuclear spin properties and conventions for chemical shifts - IUPAC recommendations 2001, *Solid State Nucl. Magn. Reson.*, 2002, **22**, 458–483.
24 C. Lin, *et al.*, Crystallization behavior of $80GeS_2{\cdot}20Ga_2S_3$ chalcogenide glass, *Appl. Phys. A*, 2009, **97**, 713–720.
25 M. Rozé, *et al.*, Optical and Mechanical Properties of Glasses and Glass-Ceramics Based on the Ge-Ga-Se System, *J. Am. Ceram. Soc.*, 2008, **91**, 3566–3570.
26 A. Yang, *et al.*, Ga–Sb–S Chalcogenide Glasses for Mid–Infrared Applications, *J. Am. Ceram. Soc.*, 2016, **99**, 12–15.
27 A. Lecomte, V. Nazabal, D. L. Coq and L. Calvez, Ge-free chalcogenide glasses based on Ga-Sb-Se and their stabilization by iodine incorporation, *J. Non-Cryst. Solids*, 2018, **481**, 543–547.

